



Cite this: *Nanoscale*, 2019, **11**, 21782

## Hybrid nanovaccine for the co-delivery of the mRNA antigen and adjuvant†

Jingnan Yang,<sup>‡a</sup> Smriti Arya,<sup>‡b</sup> Pingsai Lung,<sup>a</sup> Qiubin Lin,<sup>b</sup> Jiandong Huang<sup>\*b</sup> and Quan Li  <sup>\*a</sup>

For efficient cancer vaccines, the antitumor function largely relies on cytotoxic T cells, whose activation can be effectively induced *via* antigen-encoding mRNA, making mRNA-based cancer vaccines an attractive approach for personalized cancer therapy. While the liposome-based delivery system enables the systemic delivery and transfection of mRNA, incorporating an adjuvant that is non-lipid like remains challenging, although the co-delivery of mRNA (antigen) and effective adjuvant is key to the activation of the cytotoxic T cells. This is because the presence of an adjuvant is important for dendritic cell maturation—another necessity for cytotoxic T cell activation. In the present work, we designed a poly (lactic-co-glycolic acid) (PLGA)-core/lipid-shell hybrid nanoparticle carrier for the co-delivery of mRNA and gardiquimod (adjuvant that cannot be incorporated into the lipid shell). We demonstrated in the present work that the co-delivery of mRNA and gardiquimod led to the effective antigen expression and DC maturation *in vitro*. The intravenous administration of the hybrid nanovaccine resulted in the enrichment of mRNA expression in the spleen and a strong immune response *in vivo*. The simultaneous delivery of the antigen and adjuvant both spatially and temporally *via* the core/shell nanoparticle carrier is found to be beneficial for tumor growth inhibition.

Received 28th June 2019,  
Accepted 24th September 2019

DOI: 10.1039/c9nr05475h

rsc.li/nanoscale

## Introduction

Cancer vaccines represent an important branch of cancer immunotherapy. The choice of antigen in cancer vaccines is critical, as it mounts the initial stimulation to the immune system. Among various choices of antigens, the mRNA antigen is the most employed one, as it has been found to induce a strong major histocompatibility complex (MHC) I-mediated CD8<sup>+</sup> T cell (also known as cytotoxic T cell) response, being crucial to bringing the antitumor function for personalized cancer vaccines.<sup>1,2</sup> However, effective mRNA delivery is not an easy task. The intracellular transfection of mRNA to an effective antigen is a pre-requisite for antigen presentation in dendritic cells (DCs).<sup>3</sup> The negative charge of mRNA and lack of targeting function make it difficult for its cellular uptake.<sup>2</sup> Moreover, the easy degradation of mRNA by ubiquitous nucleases limits the methods of administration *in vivo*.<sup>2,3</sup> In most cases, systemic mRNA delivery using intravenous (i.v.)

administration has to be avoided,<sup>4,5</sup> although i.v. injection could result in the spleen enrichment of the vaccine, being favorable for DC targeting and DC-T cell communication for the enhanced vaccination effect.<sup>5,6</sup> To tackle the above outstanding issues, much effort has been devoted to developing carrier systems for mRNA delivery,<sup>6–9</sup> and lipid-based nanomaterials are found to be the most effective one. The effective packaging of mRNA by liposome-based materials indeed provides protection against mRNA degradation and facilitates its cellular uptake. It also meets the requirement of cytosolic delivery for effective transfection to ensure the desired antigen presentation.<sup>4,10</sup>

Other than effective antigen presentation, the desired polarization of T helper cells and activation of effector T cells (CD 8<sup>+</sup> T cells) also require the presence of “danger signals”, usually provided by the adjuvant, the main function of which is to stimulate the maturation of dendritic cells.<sup>11</sup> In this regard, the delivery of the adjuvant and mRNA together is considered important. One shall note that timing is important in such delivery, as the arrival of the adjuvant in DCs earlier than the antigen would cause DC pre-maturation, inhibiting the DC’s capability of antigen uptake, and thus being detrimental to the vaccination.<sup>6</sup> On the other hand, the choice of adjuvant is not random. Toll-like receptor (TLR) ligands have been known as one class of promising potent adjuvants for anti-cancer immunotherapy. In cancer vaccines, a more polarized

<sup>a</sup>Department of Physics, The Chinese University of Hong Kong, Shatin, New Territories, Hong Kong. E-mail: liquan@phy.cuhk.edu.hk

<sup>b</sup>School of Biomedical Sciences, The University of Hong Kong, Hong Kong. E-mail: jdhuang@hku.hk

†Electronic supplementary information (ESI) available. See DOI: 10.1039/c9nr05475h

‡These authors contributed equally.

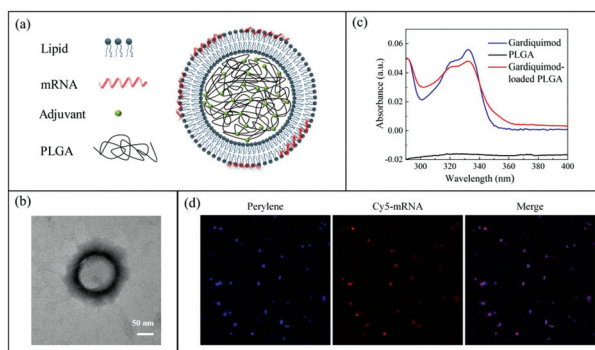


**Fig. 1** (a) Schematic illustration of the hybrid nanoparticles for the co-delivery of mRNA and adjuvant. (b) TEM image disclosing the morphology of lipid-coated PLGA hybrid nanoparticles. (c) UV-VIS spectrum of gardiquimod-loaded PLGA, free gardiquimod and pure PLGA. (d) Fluorescence image showing the overlap between the fluorescence signal of Cy5-mRNA and perylene containing hybrid nanoparticles.

Th1 cell response is preferred, and it can be elicited by TLR3, TLR4, TLR7, TLR8 and TLR9 ligands.<sup>12,13</sup> However, the TLR8 ligand has been proposed to be expressed in humans, but not in mice, which may cause difficulties in animal models.<sup>13,14</sup> The TLR4 ligand is inefficient at eliciting the CD8<sup>+</sup> T cell response.<sup>12</sup> Thus, the TLR3, 7, and 9 ligands appear to be good adjuvant choices for cancer vaccines. The TLR 7 ligand is particularly attractive for eliciting the CD8<sup>+</sup> T cell response<sup>15–17</sup> and inducing the release of type I interferons (IFNs) for an effective T cell response and antitumor immunity.<sup>6,16</sup> Unfortunately, the liposome-based carrier system only allows easy incorporation of lipid-similar adjuvants,<sup>16–18</sup> but not other adjuvants, such as small molecules of the TLR 7 ligand.

In the present work, we adopted a hybrid nanoparticle approach in designing the co-delivery system of mRNA and TLR7 adjuvant (Fig. 1(a)). A poly (lactic-co-glycolic acid) (PLGA)-core/lipid-shell nanoparticle was developed as the carrier. The adoption of the PLGA core enabled the efficient loading of the hydrophobic TLR7 adjuvant (gardiquimod in the present work), and the lipid shell allowed the conjugation of mRNA. We demonstrated in the present work that the co-delivery of mRNA and TLR7 adjuvant led to the effective antigen expression and DC activation *in vitro*. The intravenous administration of the hybrid nanovaccine resulted in the enrichment of mRNA expression in the spleen and a strong anti-tumor immune response *in vivo*. We further showed that the co-delivery (both spatially and temporally) of the antigen and adjuvant enabled by the core/shell nanoparticle carrier is beneficial for tumor growth inhibition.

## Results and discussion

### Design of hybrid particles for adjuvant loading together with mRNA

A lipid-coated PLGA (PLGA@lipid) hybrid carrier system was designed for the co-delivery of mRNA and TLR7 adjuvant.

PLGA, a biodegradable and biocompatible drug carrier, serves as an excellent candidate for encapsulating hydrophobic adjuvants (such as gardiquimod) and at the same time allowing liposomes to reassemble onto its surface.<sup>19,20</sup> PLGA nanoparticles with ~200 nm hydrodynamic size in diameter and a zeta potential of -20 mV were obtained first. The PLGA@lipid hybrid nanoparticles were made by lipid self-organization onto the as-synthesized PLGA nanoparticles with ~300 nm hydrodynamic size in diameter and ~32 mV zeta potential (size and zeta potential comparisons of pure PLGA and PLGA/lipid can be found in Table S1†). The transmission electron microscopy (TEM) image (Fig. 1(b)) shows the representative morphology of such a hybrid particle. The presence of a dark ring (contributed by the negative staining of the lipid) suggested the core-shell structure of the hybrid system.<sup>21</sup>

Adjuvant incorporation into the PLGA nanoparticles was realized by encapsulating gardiquimod into the PLGA core *via* double emulsion. Gardiquimod-loaded PLGA also had a hydrodynamic size of ~200 nm in diameter and a zeta potential of about -20 mV (also listed in Table S1†). Both these values were similar to those of blank PLGA. The effective loading of gardiquimod into the PLGA nanoparticle was confirmed by the ultraviolet-visible (UV-VIS) absorption spectrum of gardiquimod-loaded PLGA (Fig. 1(c)). The characteristic absorption peak of gardiquimod at 333 nm was observed in such a sample. The loading efficiency of gardiquimod was estimated as  $1.41 \pm 0.03\%$  (for details, see experiments and Fig. S1†).

Further incorporation of mRNA into the lipid layer on the gardiquimod-loaded hybrid nanoparticle increased the particle size to ~400 nm but with a rather narrow size distribution. The cationic lipid/mRNA charge ratio of 3:1 led to ~20 mV zeta potential of adjuvant-loaded hybrid-mRNA (Table S1†). The morphology of the mRNA loaded hybrid NP is similar to that of the hybrid nanoparticle without gardiquimod/mRNA loading (Fig. 1(b)). To find out whether mRNA can be successfully conjugated onto the hybrid NPs, perylene (dye instead of gardiquimod) was encapsulated into the PLGA core and Cy5-mRNA was employed for the imaging purpose. The obvious overlapping between the fluorescent signals of perylene at 450 nm in the polymeric core and Cy5-mRNA at 670 nm further confirmed the formation of hybrid-mRNA nanoparticles (Fig. 1(d)).

### *In vitro* mRNA transfection of DCs by hybrid-mRNA nanoparticles

To induce an adaptive immune response, the efficient transfection of mRNA-based vaccine should be realized in antigen presentation cells (APCs), *e.g.* dendritic cells (DCs).<sup>22</sup> We therefore tested the mRNA transfection by feeding hybrid-mRNA nanoparticles to DCs (the most efficient APCs) in the presence of serum to mimic the conditions *in vivo*. The mRNA encoded with the enhanced green fluorescence protein (EGFP) gene was used for the preparation of both hybrid-mRNA and adjuvant-loaded hybrid-mRNA nanoparticles. As shown in Fig. 2(a), little fluorescence signal was found in the control group (blank). Similar results were obtained in the dendritic cells fed with

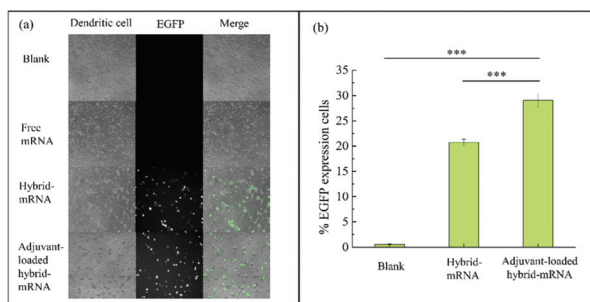


**Fig. 2** (a) Fluorescence images disclosing the EGFP mRNA transfection in DCs. (b) Flow cytometry analysis of EGFP mRNA transfection in DCs. The results are reported as mean  $\pm$  SD;  $n = 4$  and  $***p < 0.001$ .

naked EGFP mRNA, being consistent with literature reports.<sup>23</sup> This is commonly ascribed to mRNA degradation in the presence of serum nucleases when no protection of mRNA is provided.<sup>22</sup> In contrast, a strong fluorescence signal was observed in both hybrid-mRNA and adjuvant-loaded hybrid-mRNA treatments, indicating their improved transfection efficiency compared to that of naked mRNA. The quantitative results of the transfection efficiency in dendritic cells were obtained using flow cytometry (Fig. 2(b)). Here adjuvant-loaded hybrid-mRNA had the higher transfection efficiency of  $29.05 \pm 1.39\%$  when compared to hybrid-mRNA (without adjuvant loading). This result indicated that the co-delivery of mRNA and adjuvant could improve the transfection efficiency. Overall, the transfection efficiency of adjuvant-loaded hybrid-mRNA was comparable to those in the literature reports of lipid-based systems, in which transfection efficiencies from 17% to 40% were obtained.<sup>24–27</sup>

### *In vitro* activation and antigen presentation of DCs by hybrid-mRNA nanoparticles

To determine whether gardiquimod-loaded hybrid mRNA NPs could activate dendritic cells, we treated the dendritic cells with PBS, hybrid-mRNA NPs (without gardiquimod loading), and gardiquimod-loaded hybrid-mRNA NPs for 24 h. The maturation of DCs was analyzed by measuring the expression level of the maturation surface markers CD80, CD86, and CD40. As shown in Fig. 3, there was a significant upregulation in the expression levels of the activation markers CD80 (Fig. 3(a)), CD86 (Fig. 3(b)) and CD40 (Fig. 3(c)) after exposure to gardiquimod-loaded hybrid-mRNA NPs when compared to unstimulated cells (those of the PBS group are in the normal range<sup>28</sup>). The hybrid-mRNA NPs were also found to slightly increase the expression level of CD86 and CD40 (but not CD80), likely due to the self-adjuvant effect of mRNA.<sup>6</sup> Cells treated with gardiquimod-loaded hybrid-mRNA NPs showed a higher expression level of surface markers when compared to those treated with hybrid-mRNA NPs, suggesting the significantly promoted adjuvant effect after gardiquimod encapsulation in the hybrid nanocarriers.

Antigen presentation by DCs is the key for antigen-specific T cell activation. Although both MHC I and MHC II presenta-

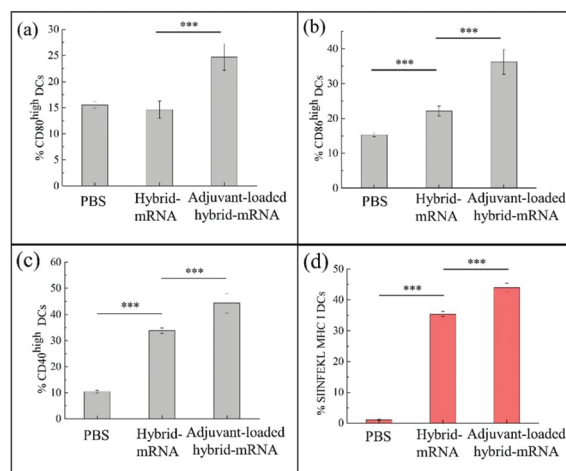


**Fig. 3** Flow cytometry analysis of CD80 (a), CD86 (b), and CD40 (c) expression on DCs, and SIINFEKL MHC I (d) expression on DCs. The results are reported as mean  $\pm$  SD,  $n = 4$ ,  $**p < 0.01$ , and  $***p < 0.001$ .

tions are involved in fully activating the antigen-specific CD8<sup>+</sup> T cell, MHC I antigen expression is the most critical. We therefore examined the expression of the ovalbumin (OVA)-derived MHC I-restricted peptide (SIINFEKL) in DCs after their treatment with different OVA-encoding mRNA complexes. The treatment groups of both hybrid-mRNA and adjuvant-loaded hybrid-mRNA have shown obvious MHC I SIINFEKL expression in DCs (Fig. 3(d)). In the adjuvant-loaded hybrid-mRNA treatment group, the frequency of DCs expressing SIINFEKL MHC I was significantly higher than those of others.

### *In vivo* transfection test

To further evaluate the transfection of mRNA *in vivo*, luciferase-encoding mRNA as a reporter gene was packaged with hybrid nanoparticles. The synthesized hybrid-mRNA and adjuvant-loaded hybrid-mRNA nanoparticles were respectively injected intravenously at the same dose of 8  $\mu$ g of mRNA. After 18 h following the luciferase mRNA injection, the mice were

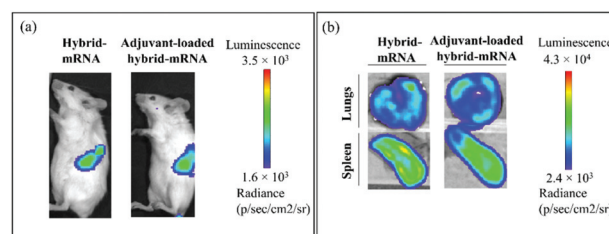


**Fig. 4** 5–6-week-old BALB/c mice were administered with hybrid-luciferase mRNA and adjuvant-loaded hybrid-luciferase mRNA complexes and after 24 hours, mice were imaged using the IVIS spectrum *in vivo* imaging system. (a) Representative whole body images of BALB/c mice after the i.v. injection of hybrid-mRNA or adjuvant-loaded hybrid-mRNA ( $n = 3$ ). (b) Representative bioluminescence imaging of isolated organs (lungs and spleen) after the i.v. injection of hybrid-mRNA or adjuvant-loaded hybrid-mRNA. Emitted photons were quantified as radiance (photons per s per cm<sup>2</sup> per sr) represented by color scale bars.

imaged. Fig. 4(a) shows the representative whole-body images of the injected mice. Both hybrid-mRNA and adjuvant-loaded hybrid-mRNA showed an intensified luminescence signal in the spleen. We then focused on comparing the expression levels of these in the isolated organs (lungs and spleen). As shown in Fig. 4(b), a luminescence signal was detected in both lungs and spleen in each sample. Both NPs had a similar expression level in the spleen, a major lymphoid organ where dense antigen presenting cells would enable efficient T cell priming and amplify T cell responses.

### *In vivo* immune response

We next carried out the *in vivo* investigation to find out whether the antigen-specific adaptive immune response could be induced by treatment with different OVA-encoding mRNA complexes. Different formulations were injected by intravenous administration at the equivalent dose of 8  $\mu\text{g}$  of OVA-encoding mRNA five times. The exact injection time point is shown in Fig. 5. After seven more days, the spleens of mice were harvested. Naïve T cells could differentiate into antigen-specific effector T cells in the spleen upon the immune response. We assessed the activation of antigen-specific effector T cells by using enzyme-linked immune absorbent spot (ELISPOT) assay to test the IFN- $\gamma$  secretion originated from CD8<sup>+</sup> T cells and CD4<sup>+</sup> T cells. Large numbers of IFN- $\gamma$  spots indicate more responsive T cells.

CD8<sup>+</sup> T cells are key to killing tumors. To assess the OVA-specific CD8<sup>+</sup> T cell response, immune cells isolated from spleens were re-stimulated with the MHC I-restricted OVA peptide (SIINFEKL). As shown in Fig. 5, the group of mice without immunization did not show any measurable number of IFN- $\gamma$  spots. In contrast, all of the mice vaccinated showed evident IFN- $\gamma$  spots, indicating the effective activation of OVA-specific CD8<sup>+</sup> T cells. In different treatment groups, a significantly higher amount of IFN- $\gamma$  secretion was observed in adjuvant-loaded hybrid-mRNA, when compared to the mice treated

with hybrid-mRNA. This result demonstrated that adjuvant-loaded hybrid-mRNA induced a stronger OVA-specific CD8<sup>+</sup> T cell immune response than hybrid-mRNA.

Although CD4<sup>+</sup> T cells are not involved directly in killing the tumors, the literature reported that simultaneous activation of CD4<sup>+</sup> T cells promoted the priming of CD8<sup>+</sup> T cells and induced a stronger anti-tumor response.<sup>29</sup> Here we also used OVA proteins to re-stimulate splenocytes for measuring IFN- $\gamma$  secretion mainly originated from OVA-specific CD4<sup>+</sup> T cells, because OVA proteins internalized into the endosome of DCs usually went through the MHC II pathway for the activation of CD4<sup>+</sup> T cells.<sup>3</sup> Similar to the OVA-specific CD8<sup>+</sup> T cell response, a few IFN- $\gamma$  spots were observed in the group of mice without treatment whereas obvious IFN- $\gamma$  spots were obtained in the immunized mice, suggesting the effective activation of OVA-specific CD4<sup>+</sup> T cells (Fig. 5). When compared to hybrid-mRNA, the number of IFN- $\gamma$  spots of adjuvant-loaded hybrid-mRNA was significantly higher than that of hybrid-mRNA. This result indicated that adjuvant-loaded hybrid-mRNA also had a stronger OVA-specific CD4<sup>+</sup> T cell immune response than hybrid-mRNA (Fig. 5). In evaluating the IFN- $\gamma$  spots, significant contribution from other kinds of immune cells such as NK cells can be excluded, as they often lack antigen-specific cell surface receptors. We also compared the group with re-stimulation and without re-stimulation. IFN- $\gamma$  spots are not detectable in all groups without re-stimulation, suggesting that the effect of other immune cells on secreting IFN- $\gamma$  spots was weak.

All treatment groups have shown simultaneous activation of OVA-specific CD4<sup>+</sup> T cells and CD8<sup>+</sup> T cells. Adjuvant-loaded hybrid-mRNA vaccination elicited a stronger immune response of both OVA-specific CD4<sup>+</sup> T cells and CD8<sup>+</sup> T cells than hybrid-mRNA, mainly due to the incorporation of the adjuvant.

### Tumor challenge

To evaluate the potential antitumor effect, we investigated both the protective and therapeutic efficacy of OVA-encoding mRNA vaccination by using the B16-OVA melanoma tumor mouse model. In addition to two formulations of hybrid-mRNA and gardiquimod-loaded hybrid-mRNA, one additional formulation using the physical mixture of hybrid-mRNA and free gardiquimod was introduced to examine the possible benefit gained from the co-delivery (both spatially and temporally) of the antigen and adjuvant. In the therapeutic model, mice were inoculated subcutaneously with B16-OVA melanoma cells first and vaccinated with different formulations at specific days shown in Fig. 6(a). From day 22 after the tumor inoculation, all groups began to show palpable tumors. Up to day 28 (the next day after the last immunization), the only gardiquimod-loaded hybrid-mRNA treated group showed obviously delayed tumor growth when compared with the control group. On day 30, all vaccinated groups have significantly smaller tumor size than the control group. When compared with the hybrid-mRNA group, a significant difference in tumor size was observed in the gardiquimod-loaded hybrid-mRNA group ( $p < 0.0001$ ) and the hybrid-mRNA plus free gardiquimod

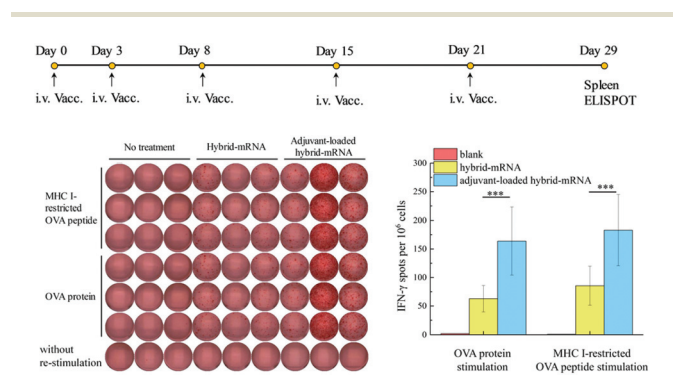


**Fig. 5** Vaccination scheme and IFN- $\gamma$  ELISPOT assay of splenocytes after *ex vivo* restimulation with the MHC-I restricted peptide (SIINFEKL) and OVA protein respectively on day 29. 5–6-week-old C57BL/6J mice were intravenously administered with OVA-mRNA-hybrid and OVA-mRNA-adjuvant-loaded hybrid complexes on days 0, 3, 8, 15 and 21. 8  $\mu\text{g}$  of OVA mRNA was used for each delivery and on day 29, and the spleen of the mice was collected to perform ELISPOT. \*\*\* $p < 0.001$ , analyzed by two-tailed unpaired Student's *t*-test ( $n = 3$ ).

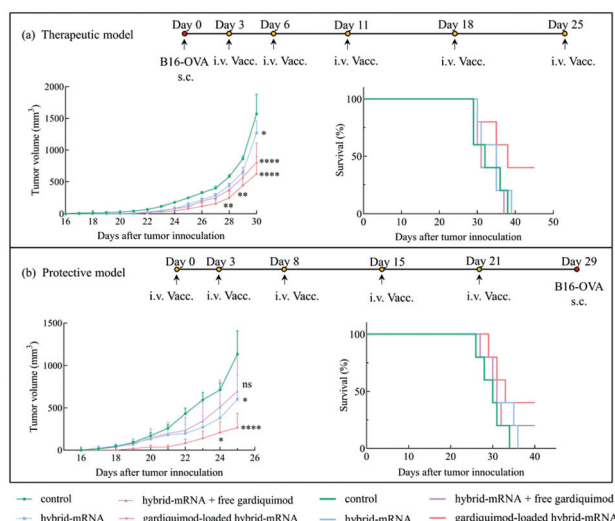


**Fig. 6** 5–6-week-old C57BL/6J mice were challenged with B16-OVA tumor subcutaneously on their right flank and were then vaccinated with OVA-encoding mRNA complexes for therapeutic vaccination, while for prophylactic vaccination, mice were vaccinated first with OVA-encoding mRNA complexes and on day 29 they were challenged with the tumor subcutaneously. (a) Tumor growth and survival rate in the therapeutic model. (b) Tumor growth and survival rate in the protective model. In the tumor growth curve, data are expressed as mean  $\pm$  SEM (ns, no significance, \* $p$  < 0.05, \*\*\* $p$  < 0.001, compared with the control group, two-way ANOVA with Bonferroni *post hoc*) ( $n$  = 5).

group ( $p$  < 0.001) respectively. The representative tumor images in the therapeutic model are included in SI Fig. 3(a).† All mice in control, hybrid-mRNA and hybrid-mRNA plus free gardiquimod groups died within 40 days. Two mice in the gardiquimod-loaded hybrid-mRNA group without the appearance of visible tumor survived for 50 days (the end of the study).

In the protective model, mice were inoculated subcutaneously with B16-OVA melanoma cells seven days after the last immunization as illustrated in Fig. 6(b). On day 19 after the tumor inoculation, the gardiquimod-loaded hybrid-mRNA treated group started to show tumor growth, while the control group and other treatment groups showed visible tumor from day 17. From day 24, the gardiquimod-loaded hybrid-mRNA treated group showed significantly delayed tumor growth when compared with the control group. On day 25, both gardiquimod-loaded hybrid-mRNA ( $p$  < 0.0001) and hybrid-mRNA ( $p$  < 0.05) groups have significantly smaller tumor size than the control group. In contrast, the hybrid-mRNA plus free gardiquimod group did not show delayed tumor growth until day 25. The representative tumor images in the protective model are shown in SI Fig. 3(b).† The death of mice in control and hybrid-mRNA groups started from day 26, and all of the mice died within 36 days. The death of mice in hybrid-mRNA plus free gardiquimod and gardiquimod-loaded hybrid-mRNA groups occurred on day 27 and day 29 respectively. The respective survival rates in the hybrid-mRNA plus free gardiquimod group and the gardiquimod-loaded hybrid-mRNA group were 20% and 40% until day 40.

The gardiquimod-loaded hybrid-mRNA group showed significantly delayed tumor growth in the therapeutic as well as the protective model. The survival rates of the gardiquimod-loaded hybrid-mRNA group were always higher than those of the hybrid-mRNA plus free gardiquimod group in both therapeutic and protective models, suggesting the possible benefit from the spatial and temporal overlap of adjuvant and antigen co-delivery.

## Conclusions

The co-delivery of mRNA and adjuvant was achieved by the PLGA-core/lipid-shell hybrid nanoparticle system, where PLGA allowed the adjuvant incorporation in the core, and the lipid shell loaded the mRNA *via* an electrostatic interaction. Although the concept of multi-modality co-delivery has been proposed earlier,<sup>3,30</sup> and there have been many attempts to develop viable nanoplatforms for multi-functionality delivery,<sup>31</sup> here we demonstrated the co-delivery of mRNA and non-lipid like adjuvant for the first time. Potentially this design can be extended to other co-delivery system designs, as PLGA allows versatile types of adjuvants to be incorporated. Enhanced antigen expression and DC maturation were demonstrated *in vitro* when using such hybrid nanoparticles to co-deliver the mRNA and the adjuvant. A stronger antigen-specific immune response was obtained by the intravenous administration of the hybrid nanovaccine containing both mRNA and TLR7 adjuvant than in those containing mRNA only. The anti-tumor effect of the hybrid nanovaccine was further demonstrated in both therapeutic and protective models employing B16-OVA. The spatial/temporal overlap of antigen and adjuvant co-delivery shows some benefit in the present work, but the significance is likely to rely on the respective pharmacokinetic features of the specific adjuvant and nanoparticle used in the nanovaccine.

## Experimental section

### Mice and cell culture

C57BL/6J mice (5–6 weeks) and Balb/c mice (5–6 weeks) were obtained from the laboratory animal unit of the University of Hong Kong (HKU). This study was performed in strict accordance with the HKU Research Ethics guidelines for the care and use of laboratory animals (HK Government Legislation Cap 340 and 169 Rev. 2017) and was approved by the Committee on the Use of Live Animals in Teaching and Research (CULATR).

To generate bone marrow-derived DCs (BMDCs), primary murine bone marrow cells were collected first. To start a culture of BMDCs, bone marrow cells were thawed and immersed in 6 mL of RPMI 1640 medium (Life technology). The collected bone marrow cells ( $\sim 10^7$  cells) were cultured in a 75 cm<sup>2</sup> non-treated flask using 10 mL of RPMI 1640 medium supplemented with 10% fetal bovine serum (FBS) (Life techno-

logy), 1% penicillin (Life technology), and 20 ng mL<sup>-1</sup> of granulocyte-macrophage colony-stimulating factor (GM-CSF) (*In vivo* gene) that was used to promote the differentiation of the monocytes into BMDCs. Cells were maintained in a humidified 5% CO<sub>2</sub> incubator at 37 °C. On day 3 of the culture, an additional 10 mL of culture medium was added. After four more days, non-adherent and loosely adherent cells were harvested and used for the experiments as immature DCs.

### Nanoparticle formulation

Liposomes composed of cationic lipid DOTAP (1,2-dioleoyl-3-trimethylammonium-propane (chloride salt), Avanti Polar Lipids) and DOPE (1,2-dioleoyl-*sn*-glycero-3-phosphoethanolamine, Avanti Polar Lipids) were synthesized by the thin film rehydration method. Lipid solutions of DOTAP and DOPE were mixed in an intended weight ratio of 3 : 1. The solvent was evaporated *via* nitrogen flow to form lipid films and the obtained lipid film was further dried under vacuum. The dry film was rehydrated with RNase-free water, which was shaken gently overnight at 4 °C.

Dye-loaded poly (lactic-*co*-glycolic acid) PLGA nanoparticles were formed *via* the oil/water (o/w) single emulsion method. Briefly, 100 mg of PLGA and 1 mg of perylene were co-dissolved in 2.5 mL of mixed solvent of 1.5 mL of dichloromethane (DCM) and 1 mL of acetone. The mixture was added to 10 mL of 5% (w/v) polyvinyl alcohol (PVA) solution dropwise under stirring. The solution was then sonicated for 6 min to generate emulsion. The organic solvent was further evaporated under stirring overnight at room temperature. Dye-loaded PLGA nanoparticles were collected and washed with distilled water by centrifugation and passed through a 0.45 μm glass fiber filter (GE) to obtain uniform size. The nanoparticles were lyophilized and stored at 4 °C for later use. Blank PLGA nanoparticles were synthesized by the same method without the addition of perylene. For gardiquimod loading, gardiquimod-loaded nanoparticles were also formed *via* the double emulsion method for higher loading efficiency.<sup>32</sup> 2.5 mg of sodium phosphate dibasic was dissolved in 500 μL of 1% (w/v) PVA aqueous phase. This aqueous phase was added dropwise to the oil phase, which consisted of 30 mg of PLGA and 3 mg of gardiquimod co-dissolved in 2 mL of chloroform. The mixture was sonicated by using an ultrasonic tip for 6 min to generate the first emulsion. The w/o emulsion was further added to 8 mL of 2% (w/v) PVA to form w/o/w emulsion and the following steps were also the same as the synthesis of dye-loaded PLGA nanoparticles.

For PLGA@lipid hybrid nanoparticle formulation, PLGA nanoparticles were firstly resuspended in RNase-free water. PLGA nanoparticle suspensions were mixed with formulated liposome solution at a weight ratio of 0.75/1 (liposome/PLGA). The mixture was incubated for 30 min to obtain PLGA@lipid hybrid nanoparticles. mRNA-incorporated nanoparticles were synthesized following ref. 6. The complex was formed *via* electrostatic attraction between the lipid and mRNA. So the N/P ratio (also defined as the charge ratio) was calculated from

the number of positive charges from the amine groups of the cationic lipid to that of negative charges from the phosphodiester groups of mRNA. They are formed by diluting mRNA with H<sub>2</sub>O and 1.5 M NaCl followed by adding various amounts of nanoparticle suspensions to reach the selected N/P ratio of 3 : 1 at a final NaCl concentration of 150 mM.

### Nanoparticle characterization

The concentration and actual ratio of DOTAP and DOPE were determined by high performance liquid chromatography (HPLC) with an ultraviolet-visible detector at 205 nm referred to the literature.<sup>33</sup> All size and zeta potential measurements were determined at 25 °C by dynamic light scattering (DLS) on a Nanosight at a diluted concentration. Each sample had three measurements with more than 10 runs.

The morphology of the hybrid structure was disclosed by TEM. The TEM sample was stained with 2% phosphotungstic acid at 10 min for better imaging contrast. The fluorescence image disclosing the overlay of mRNA and hybrid NPs was measured by using a NIKON super resolution microscope.

For the encapsulation and loading efficiency of mRNA estimation, the amount of unencapsulated mRNA was determined by using a Nanodrop to measure the mRNA concentration in the supernatant of hybrid-mRNA nanoparticles after ultracentrifugation. The encapsulation efficiency and loading efficiency were estimated to be around 91% and 4.6% respectively, which were based on the following respective equations: encapsulation efficiency = (1 – weight of the unencapsulated mRNA/weight of total mRNA added) × 100% and loading efficiency = weight of the encapsulated mRNA/weight of hybrid-mRNA nanoparticles × 100%. For the loading efficiency of adjuvant estimation, the sample of gardiquimod-loaded PLGA was dissolved in dimethyl sulfoxide (DMSO) and measured by using UV-VIS spectra to obtain the absorption peak intensity of gardiquimod. Based on the standard equation, the amount of gardiquimod was acquired (Fig. S11†). The loading efficiency (LE) is determined as the LE = weight of gardiquimod/total weight of gardiquimod-loaded PLGA.

### *In vitro* transfection test

Enhanced green fluorescence protein (EGFP)-encoding mRNA and Cy5-labeled EGFP mRNA (Trilink) were employed to assemble with hybrid nanoparticles for the *in vitro* transfection efficiency test. For the transfection test of bone-marrow derived dendritic cells (BMDCs), BMDCs were transferred into a 50 mL tube with a culture medium (RPMI medium supplemented with 10% fetal bovine serum and 1% penicillin) permitting gas exchange. The hybrid-mRNA NPs and adjuvant-loaded hybrid-mRNA at the same amount of mRNA were respectively added to the cells. After 24 h of incubation, cells were collected and washed with PBS for flow cytometry or reseeded in a 96-well plate for fluorescence microscopy imaging.

### *In vitro* maturation and antigen presentation

BMDCs were cultured in a 50 mL tube. PBS (negative control), hybrid-mRNA NPs (without an adjuvant, 59.5 μg mL<sup>-1</sup>), and

gardiquimod-loaded hybrid-mRNA NPs ( $59.5 \mu\text{g mL}^{-1}$ , equivalent to  $0.2 \mu\text{g mL}^{-1}$  of free gardiquimod) were added to each tube. After 24 h, BMDCs were collected and stained with CD40-PE, CD86-FITC, and CD80-PE Cy5. After additional washing steps, the cells were re-suspended in PBS to analyze DC maturation by flow cytometry using an S3e cell sorter. To assess MHC I antigen presentation, hybrid-mRNA and gardiquimod-loaded hybrid-mRNA at the same dose of  $5 \mu\text{g}$  of mRNA-OVA were added to each tube. After 24 h, BMDCs were harvested and stained with the anti-OVA<sub>257–264</sub> peptide bound to the H-2K<sup>b</sup>-PE antibody. The cells were washed and re-suspended in PBS to test the OVA-specific MHC I presentation by flow cytometry. All data were analyzed by using FlowJo software. The significance between two groups was determined by using the unpaired two-tailed Student *t*-test.

### *In vivo* bioluminescence imaging

Firefly luciferase (Luc)-encoding mRNA-incorporated NPs were prepared for the *in vivo* transfection test. Synthesized nanoparticles were injected intravenously at the same dose of  $8 \mu\text{g}$  of luciferase mRNA per mouse (Balb/c mice). After 18 h of luciferase mRNA injection, mice were anaesthetised first and prepared for bioluminescence *in vivo* imaging. Subsequently, luciferin was administered intraperitoneally in a volume of  $200 \mu\text{l}$  ( $15 \text{mg mL}^{-1}$ ) per mouse. After 3 min, bioluminescence images were acquired by using the IVIS system with an exposure time of 5 min. For acquiring the bioluminescence images of the separated organs, after 2 min following the luciferin injection, mice were sacrificed, and spleen and lungs were harvested.

### *In vivo* immune response

The C57BL/6J mice of age 5–6 weeks were grouped into three groups ( $n = 3$ ). The mice in the control group remained untreated. Other three groups were immunized with different formulations. Hybrid-mRNA and gardiquimod-loaded hybrid-mRNA at the same dose of  $8 \mu\text{g}$  of mRNA-OVA were injected intravenously on indicated time points, day 0, day 3, day 8, day 15 and day 22. The spleen of mice was harvested seven days after the last immunization for ELISPOT analysis. Splenocytes were extracted by milling the spleen and then dealt with lysis buffer to remove the red blood cells.  $10^6$  freshly isolated splenocytes were incubated with the MHC I-restricted peptide (SIINFEKL) and OVA protein respectively in the microtiter plate coated with the anti-IFN- $\gamma$  antibody. After 18 hours of incubation, the secondary antibody was added. The streptavidin binding was added after one more hour to wait for the spot's coloration. Finally, the IFN- $\gamma$  spots were counted using an ELISPOT plate reader.

### Tumor models

In tumor challenge, B16-OVA cells gifted by the lab of Professor Liu Zhuang were employed as the tumor model. In the therapeutic model, B16-OVA cells ( $10^5$ ) were inoculated subcutaneously on the right flank in C57BL/6J mice first. After three days, mice were immunized as per the previous protocol. In the protective model, C57BL/6J mice were immunized as

per the previous protocol first. After additional seven days, B16-OVA cells ( $2 \times 10^5$ ) were inoculated subcutaneously. Once the tumor became palpable, the tumor size was measured with a caliper. The tumor area was calculated using the following equation: width  $\times$  length.

### Statistical analysis

The results were presented as the mean  $\pm$  standard deviation (SD) or mean  $\pm$  standard error of the mean (SEM). The unpaired two-tailed Student *t*-test was used for comparisons of two groups. Two-way ANOVA with the Bonferroni *post-hoc* test was used when both time and treatment were considered. The survival rate was analyzed with the log-rank test. Statistical analysis was performed with GraphPad Prism software ( $*p < 0.05$ ,  $**p < 0.01$ ,  $***p < 0.001$ , and  $****p < 0.0001$ ).

### Conflicts of interest

There are no conflicts to declare.

### Acknowledgements

The authors are grateful for financial support from the HMRP under project no. 18170262. This study was also supported by the Shenzhen Peacock project (KQTD2015033117210153) and the Shenzhen Science and Technology Innovation Committee Basic Science Research Grant (JCYJ20170413154523577). We also thank Wenlong Zuo and Yilin Wu for the assistance with fluorescence microscopy imaging and Jun Xu and Zhuang Liu for kindly providing B16-OVA cells.

### References

- 1 C. J. M. Melief, T. van Hall, R. Arens, F. Ossendorp and S. H. van der Burg, *J. Clin. Invest.*, 2015, **125**, 3401–3412.
- 2 U. Sahin, K. Karikó and Ö. Türeci, *Nat. Rev. Drug Discovery*, 2014, **13**, 759.
- 3 G. Zhu, F. Zhang, Q. Ni, G. Niu and X. Chen, *ACS Nano*, 2017, **11**, 2387–2392.
- 4 K. A. Hajj and K. A. Whitehead, *Nat. Rev. Mater.*, 2017, **2**, 17056.
- 5 S. Uchida, H. Kinoh, T. Ishii, A. Matsui, T. A. Tockary, K. M. Takeda, H. Uchida, K. Osada, K. Itaka and K. Kataoka, *Biomaterials*, 2016, **82**, 221–228.
- 6 L. M. Kranz, M. Diken, H. Haas, S. Kreiter, C. Loquai, K. C. Reuter, M. Meng, D. Fritz, F. Vascotto, H. Hefesha, C. Grunwitz, M. Vormehr, Y. Hüsemann, A. Selmi, A. N. Kuhn, J. Buck, E. Derhovanessian, R. Rae, S. Attig, J. Diekmann, R. A. Jabulowsky, S. Heesch, J. Hassel, P. Langguth, S. Grabbe, C. Huber, Ö. Türeci and U. Sahin, *Nature*, 2016, **534**, 396.
- 7 R. W. Malone, P. L. Felgner and I. M. Verma, *Proc. Natl. Acad. Sci. U. S. A.*, 1989, **86**, 6077.

- 8 A. Akinc, M. Thomas, A. M. Klivanov and R. Langer, *J. Gene Med.*, 2005, **7**, 657–663.
- 9 O. Boussif, F. H. Lezoualc, M. A. Zanta, M. D. Mergny, D. Scherman, B. Demeneix and J. P. Behr, *Proc. Natl. Acad. Sci. U. S. A.*, 1995, **92**, 7297.
- 10 S. Rietwyk and D. Peer, *ACS Nano*, 2017, **11**, 7572–7586.
- 11 M. S. Goldberg, *Cell*, 2015, **161**, 201–204.
- 12 R. L. Coffman, A. Sher and R. A. Seder, *Immunity*, 2010, **33**, 492–503.
- 13 S. G. Reed, M. T. Orr and C. B. Fox, *Nat. Med.*, 2013, **19**, 1597.
- 14 L. Nuhn, N. Vanparijs, A. De Beuckelaer, *et al.*, *Proc. Natl. Acad. Sci. U. S. A.*, 2016, **113**, 8098–8103.
- 15 F. Heil, H. Hemmi, H. Hochrein, F. Ampenberger, C. Kirschning, S. Akira, G. Lipford, H. Wagner and S. Bauer, *Science*, 2004, **303**, 1526.
- 16 M. A. Oberli, A. M. Reichmuth, J. R. Dorkin, M. J. Mitchell, O. S. Fenton, A. Jaklenec, D. G. Anderson, R. Langer and D. Blankschtein, *Nano Lett.*, 2017, **17**, 1326–1335.
- 17 R. Verbeke, I. Lentacker, L. Wayteck, K. Breckpot, M. Van Bockstal, B. Descamps, C. Vanhove, S. C. De Smedt and H. Dewitte, *J. Controlled Release*, 2017, **266**, 287–300.
- 18 R. Verbeke, I. Lentacker, K. Breckpot, J. Janssens, S. Van Calenbergh, S. C. De Smedt and H. Dewitte, *ACS Nano*, 2019, **13**, 1655–1669.
- 19 S. Tan, X. Li, Y. Guo and Z. Zhang, *Nanoscale*, 2013, **5**, 860–872.
- 20 A.-L. Troutier, L. Véron, T. Delair, C. Pichot and C. Ladavière, *Langmuir*, 2005, **21**, 9901–9910.
- 21 L. Zhang, J. M. Chan, F. X. Gu, J.-W. Rhee, A. Z. Wang, A. F. Radovic-Moreno, F. Alexis, R. Langer and O. C. Farokhzad, *ACS Nano*, 2008, **2**, 1696–1702.
- 22 K. A. Hajj, *Nat. Rev. Mater.*, 2017, **2**, 17056.
- 23 X. Su, J. Fricke, D. G. Kavanagh and D. J. Irvine, *Mol. Pharm.*, 2011, **8**, 774–787.
- 24 R. Verbeke, I. Lentacker, L. Wayteck, *et al.*, *J. Controlled Release*, 2017, **266**, 287–300.
- 25 X. Su, J. Fricke, D. G. Kavanagh, *et al.*, *Mol. Pharm.*, 2011, **8**, 774–787.
- 26 A. S. Irvine, P. K. E. Trinder, D. L. Laughton, *et al.*, *Nat. Biotechnol.*, 2000, **18**, 1273.
- 27 S. Awasthi and R. A. Cox, *BioTechniques*, 2003, **35**, 600–604.
- 28 H. Kim, L. Niu, P. Larson, T. A. Kucaba, K. A. Murphy, B. R. James, D. M. Ferguson, T. S. Griffith and J. Panyam, *Biomaterials*, 2018, **164**, 38–53.
- 29 K. Palucka and J. Banchereau, *Nat. Rev. Cancer*, 2012, **12**, 265.
- 30 R. Kuai, L. J. Ochyl, K. S. Bahjat, A. Schwendeman and J. J. Moon, *Nat. Mater.*, 2016, **16**, 489.
- 31 R. Xing, G. Liu, Q. Quan, A. Bhirde, G. Zhang, A. Jin, L. H. Bryant, A. Zhang, A. Liang, H. S. Eden, Y. Hou and X. Chen, *Chem. Commun.*, 2011, **47**, 12152–12154.
- 32 H. Kim, D. Sehgal, T. A. Kucaba, D. M. Ferguson, T. S. Griffith and J. Panyam, *Nanoscale*, 2018, **10**, 20851–20862.
- 33 O. Meyer, O. Roch, D. Elmlinger, *et al.*, *Eur. J. Pharm. Biopharm.*, 2000, **50**, 353–356.